Theor. Comput. Fluid Dyn. (2022) 36:423–433
https://doi.org/10.1007/s00162-021-00602-x

ORIGINAL ARTICLE

Hyundong Kim · Junxiang Yang · Sangkwon Kim · Chaeyoung Lee · Sungha Yoon · Soobin Kwak · Junseok Kim

Numerical simulation of the coffee-ring effect inside containers with time-dependent evaporation rate

Received: 16 July 2021 / Accepted: 27 December 2021 / Published online: 6 January 2022

Abstract In this work, using a mathematical model and numerical simulation, we investigate the effect of time-dependent evaporation rates on stripe formation inside containers. This pattern formation is driven by the coffee-ring effect. The coffee particles inside a container move according to random walk and under the gravitational force. Because of the time-dependent evaporation rate, we can observe stripe formation inside a container after evaporation of the coffee particle-laden liquid. Various numerical experiments are performed to demonstrate the proposed model can simulate the stripe formation in a container.

Keywords Stripe formation · Time-dependent evaporation rate · Coffee-ring effect

1 Introduction

When a drop of coffee evaporates on a solid substrate, the coffee particles form a ring-like stain at the contact line. This phenomenon is a consequence of faster evaporation at the contact line, driving the coffee particles to convectively migrate toward the contact lines, which is known as the coffee-ring effect [1,2]. Figure 1a, b shows coffee droplets on a transparent film on a grid paper before and after evaporation, respectively. After evaporation of coffee droplet, we can observe the coffee-ring pattern as shown in Fig. 1b.

The physical phenomenon related to the coffee-ring effect has been researched in several experiments with various colloidal suspensions containing nanoparticles [3], air bubbles [4], biological fluids [5], and bacteria [6]. Poulichet et al. [7] showed that the coffee-ring effect can be observed without evaporation when the solvent of a drop transfers into another liquid. There are many physical applications using the principle of coffee-ring effect such as ink-jet printing [8], making crystal morphologies [9], central spot formation in droplets [10], uniform droplet printing of graphene micro-rings [11], quantitative immunoassays [12], coffee-ring effect in polymer-nanocrystal mixtures [13], and micro-technologies in biological field [14]. For more detailed review on coffee-ring effect, see [15]. The coffee-ring effect has also been investigated in various numerical experiments based on the Monte Carlo method [16–18], finite element method [19], and finite difference method [20].

Figure 2a, b, c shows photographs of coffee solution contained in a conical flask, stripe pattern after evaporation, and magnified view of a part in (b), respectively. As we can see in Fig. 2b, c, there is a stripe pattern, i.e., the coffee-ring effect is alternatively strong (thick ring) and weak (thin ring) in the vertical direction. This phenomenon happens because of time-dependent evaporation rate in room temperature. During 24 h in a day, evaporation rate keeps changing due to temperature, humidity, wind speed, and surface area, for example.

Communicated by Peter Duck.

H. Kim · J. Yang · S. Kim · C. Lee · S. Yoon · S. Kwak · J. Kim (✉)
Department of Mathematics, Korea University, Seoul 02841, Republic of Korea
E-mail: cfdkim@korea.ac.kr
H. Kim
E-mail: rlagusehd@korea.ac.kr

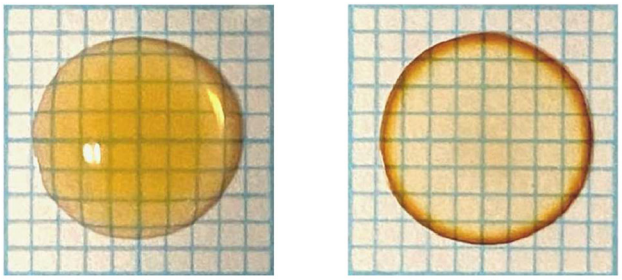

(a) (b)

Fig. 1 Coffee droplets on a transparent film on a grid paper **a** before and **b** after evaporation

(a) (b) (c)

Fig. 2 Stripe pattern from coffee-ring effect: **a** coffee solution contained in a conical flask, **b** coffee angel rings made after evaporation, and **c** magnified view of a part in **b**

Most of the previous numerical studies were performed to investigate the coffee-ring effect of evaporating drops on the substrate domain. Motivated by the stripe pattern formation phenomenon with time-dependent evaporation, the objective of the present study is to present a mathematical model which can simulate the stripe pattern formation driven by coffee-ring effect and time-dependent evaporation rate.

This paper is organized as follows. In Sect. 2, we present the governing equation and its numerical solution algorithm. The numerical results are presented in Sect. 3. Finally, conclusions are drawn in Sect. 4.

2 Governing equation and numerical solution algorithm

Let Ω_t be a time-dependent liquid domain at time t in a solid container. The time-dependent liquid domain Ω_t is defined by a level-set function (a signed distance function) $\phi(\mathbf{x}, t)$, i.e., $\Omega_t = \{\mathbf{x} \in \mathbb{R}^3 | \phi(\mathbf{x}, t) \geq 0\}$. Let $\Gamma_t = \left\{ \mathbf{x} \mid \mathbf{x} = (x, y, z^*) \in \Omega_t \text{ and } z^* = \max_{(x,y,z)\in\Omega_t} z \right\}$ be the liquid surface at time t contacting the air. The liquid domain contains the coffee particles which are defined as the Lagrangian points moving under Brownian motion and gravitational force. Figure 3a, b shows a time-dependent liquid domain Ω_t including coffee particles and a top-level surface of liquid domain Γ_t with the scalar field ϕ at time $t = 0$ and $t > 0$, respectively.

For the sake of simplicity of modeling, we assume coffee particles have only mass and no volume and the fluid surface moves under the time-dependent evaporation rates. Assuming that the force on the particle is

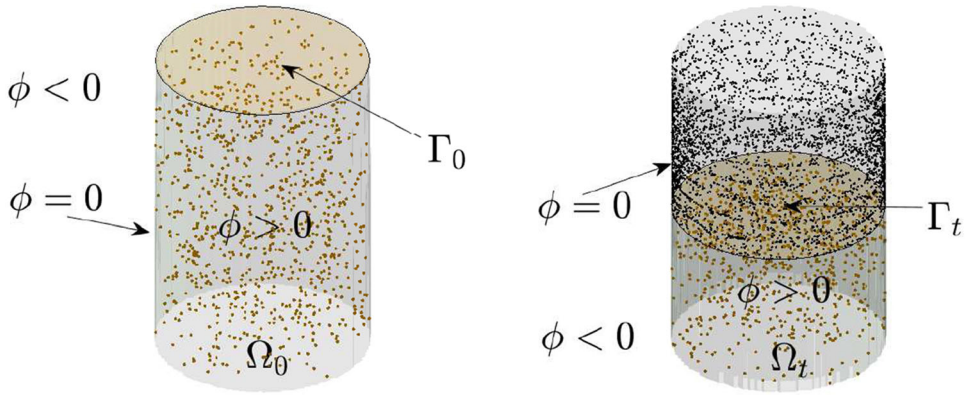

Fig. 3 Schematic illustration of the liquid domain Ω_t over time at **a** $t = 0$ and **b** $t > 0$. Note that the colored surface represents the top-level surface Γ_t

zero, the governing equation can be derived from the Langevin equation [20]:

$$\frac{\mathrm{d}\mathbf{X}}{\mathrm{d}t} = \frac{\alpha}{\sqrt{\mathrm{d}t}}\boldsymbol{\psi}(\mathbf{X}) + \mathbf{g} \text{ on } \Omega_t, \tag{1}$$

where $\mathbf{X}$ is Lagrangian variable for a particle, t is time, $\mathbf{g} = (0, 0, -g)$ is the scaled gravitational force. Here, $\boldsymbol{\psi}(\mathbf{X}) = (\rho\cos(\theta)\sin(\varphi),\ \rho\sin(\theta)\sin(\varphi),\ \rho\cos(\varphi))$ represents random force of Brownian particle, where ρ is a random variable with the probability density function $f(\rho) = e^{-0.5\rho^2}/\sqrt{2\pi}$ and between $[-3,\ 3]$ which is 99.998% confidence interval. Therefore, we can safely restrict ρ within the interval $[-3, 3]$. The random variables θ and φ are uniformly distributed on the interval $[0,\ \pi]$. Using the explicit Euler's method, we discretize Eq. (1) as

$$\frac{\mathbf{X}_k^{n+1} - \mathbf{X}_k^n}{\Delta t} = \frac{\alpha}{\sqrt{\Delta t}}\boldsymbol{\psi}(\mathbf{X}_k^n) + \mathbf{g},\quad k = 1, 2, \ldots, N_k, \tag{2}$$

where $\mathbf{X}_k^n$ is the k-th particle position at time $t = n\Delta t$, Δt is the time step, and N_k is the total number of particles. Equation (2) can be rewritten as

$$\mathbf{X}_k^{n+1} = \mathbf{X}_k^n + \alpha\sqrt{\Delta t}\boldsymbol{\psi}(\mathbf{X}_k^n) + \Delta t\mathbf{g},\quad k = 1, 2, \ldots, N_k. \tag{3}$$

Let $\mathbf{X}_k^{n+1} = (X_k^{n+1}, Y_k^{n+1}, Z_k^{n+1})$ be the $n+1$ time-level and k-th particle position computed by using the evolution equation (3). A particle becomes pinned if it satisfies the following three conditions:

(i) $\phi(\mathbf{X}_k^{n+1}, t) < 0$,
(ii) $Z_k^{n+1} > S(t)$, where $S(t)$ is the position of the liquid surface at time $t = n\Delta t$, i.e., $S(t) = \max_{(x,y,z)\in\Omega_t} z$, and
(iii) $(X_k^{n+1}, Y_k^{n+1}, S(t)) \notin \Gamma_t$.

If a particle moves outside the domain, then it goes back to fluid boundary, see the schematic representation of this process in Fig. 4. The pinning position of a pinned particle is defined as the closest point in Γ_t from $\mathbf{X}_k^{n+1}$ as illustrated with a diamond symbol. If a particle without becoming pinned goes outside the liquid domain ($\phi < 0$), then the particle moves to the closest point of $\phi = 0$, see the square and triangle symbols.

3 Numerical experiments

Unless otherwise stated, $z = S(t)$ is the position of the liquid surface at time t, the total number of particles N_k is set to 5×10^5, N_p is the number of pinned particles, the gravitational force is fixed to $\mathbf{g} = (0, 0, -1)$, and the size of bins in the histograms is set to 0.03.

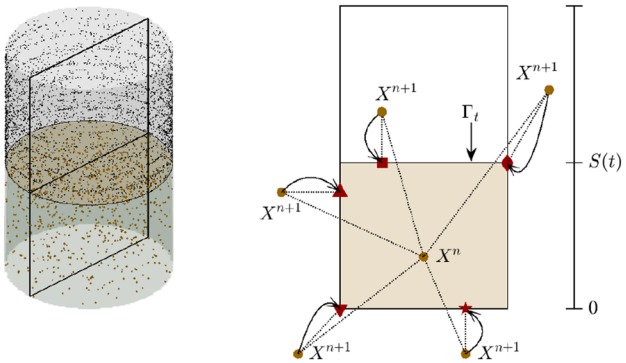

Fig. 4 Schematic representation of pinning process

3.1 Particle motion without evaporation

We first perform the numerical simulation for the motion of particles without evaporation in a cylindrical container. The static liquid domain is defined as follows:

$$\Omega_t = \left\{ \mathbf{x} \in \mathbb{R}^3 | \sqrt{x^2 + y^2} \leq 1 \text{ and } 0 \leq z \leq 3 \right\}. \tag{4}$$

Then, we can define a signed distance function as

$$\phi(\mathbf{x}, t) = \begin{cases} \text{dist}(\mathbf{x}, \partial\Omega_t) & \text{if } \mathbf{x} \in \Omega_t, \\ -\text{dist}(\mathbf{x}, \partial\Omega_t) & \text{otherwise,} \end{cases} \tag{5}$$

where $\partial\Omega_t$ is the boundary of the domain Ω_t and $\text{dist}(\mathbf{x}, \partial\Omega_t) = \min_{\mathbf{y}\in\partial\Omega_t} |\mathbf{x} - \mathbf{y}|$ is the distance function between $\mathbf{x}$ and $\partial\Omega_t$. The temporal step size $\Delta t = 0.001$ and $\alpha = 0.5$ are used. The total number of particles is $N_k = 10^5$. Because there is no evaporation, we assume there is no pinning of particles. The evolution of particles in a cylindrical container without evaporation can be seen in Fig. 5a. The number of particles with respect to height is shown in Fig. 5b. As can be seen from the histogram in Fig. 5b, particles move downward due to the gravitational force.

3.2 Coffee-ring formation with constant evaporation rate

Now, let us consider coffee-ring formation with constant evaporation rate. The time-dependent liquid domain is defined as follows:

$$\Omega_t = \left\{ \mathbf{x} \in \mathbb{R}^3 | \sqrt{x^2 + y^2} \leq 1 \text{ and } 0 \leq z \leq S(t) \right\}, \tag{6}$$

where $S(t) = 3 - 1.25t$ is the position of the liquid surface at time t and schematically illustrated in Fig. 4. Note that the evaporation rate is defined as $\mathrm{d}S(t)/\mathrm{d}t$, which is the rate of length with respect to time. Then, we can define a time-dependent signed distance function $\phi(\mathbf{x}, t)$ as described in Eq. (5). We use $\Delta t = 0.001$ and $\alpha = 1, 1.5, 2$. Figure 6a shows the evolution of particles in a cylindrical container using $\alpha = 1$. The numbers of pinned particles are shown in Fig. 6b, c, d using $\alpha = 2,\ 1.5$, and 1, respectively. We can observe the more pinned particles because the particles move farther if α is larger .

3.3 Coffee-ring formation with changing evaporation rate

Using the proposed method, we perform the numerical simulation for the stripe pattern formation in a cylindrical container with the time-dependent evaporation rate. The time-dependent liquid domain is defined as follows:

$$\Omega_t = \left\{ \mathbf{x} \in \mathbb{R}^3 | \sqrt{x^2 + y^2} \leq 1 \text{ and } 0 \leq z \leq S(t) \right\}, \tag{7}$$

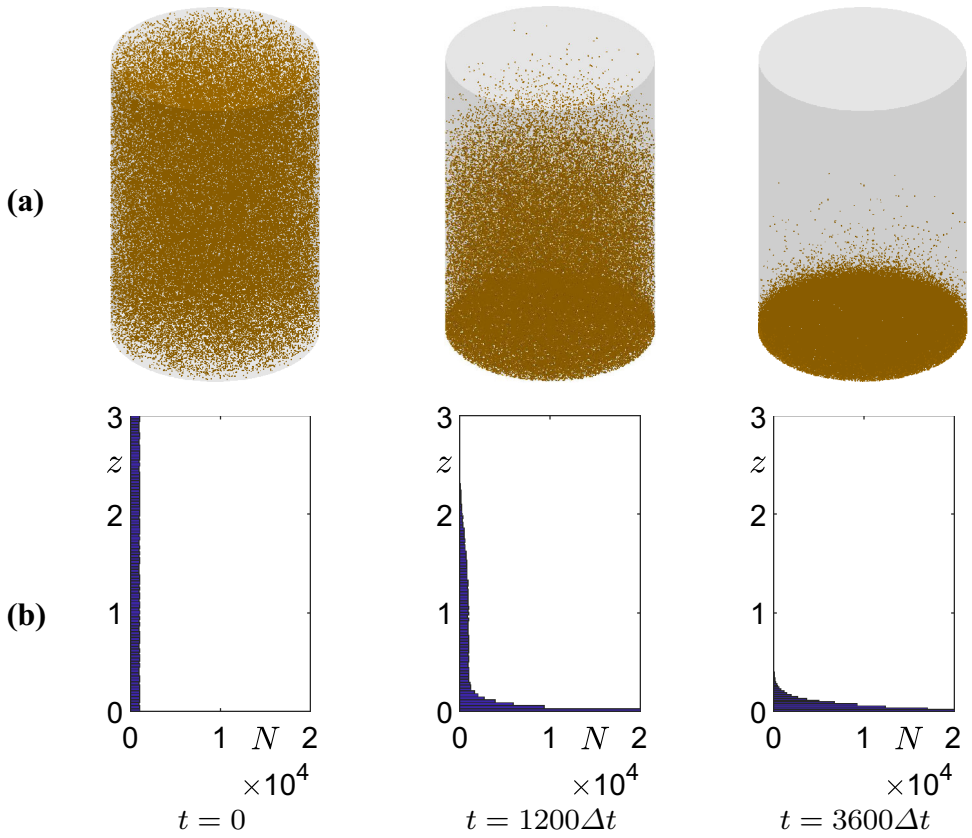

Fig. 5 **a** Evolution of particles in a cylindrical container without evaporation. **b** Histograms of particle numbers (N) with respect to height at the corresponding times

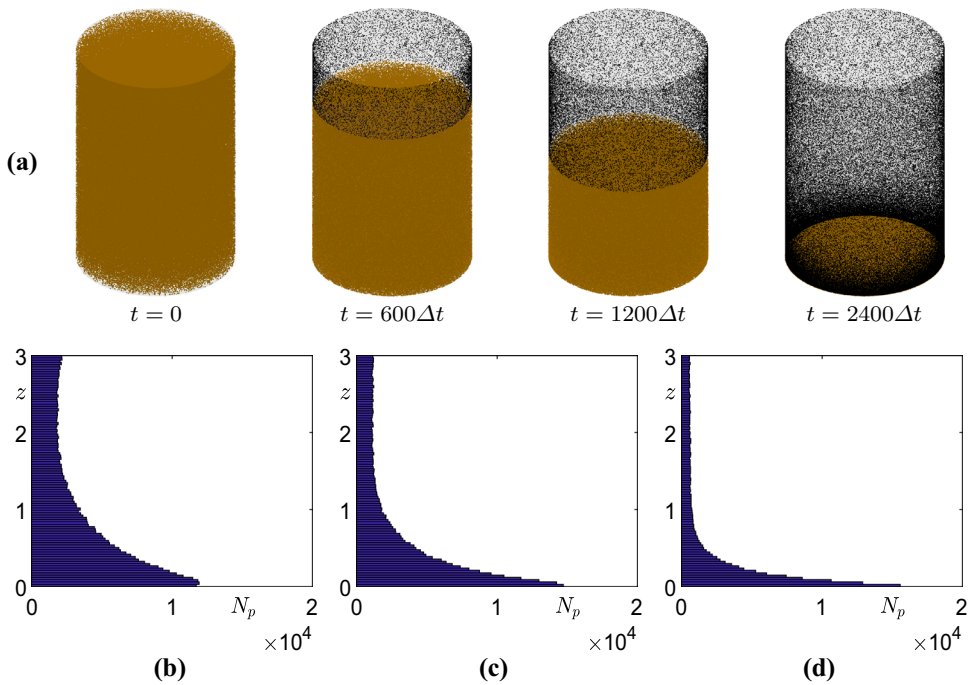

Fig. 6 **a** Evolution of particles in a cylindrical container using $\alpha = 1$. **b**, **c**, **d** Are the histograms of pinned particles with respect to height at final time $t = 2400\Delta t$ using $\alpha = 2,\ 1.5$, and 1, respectively

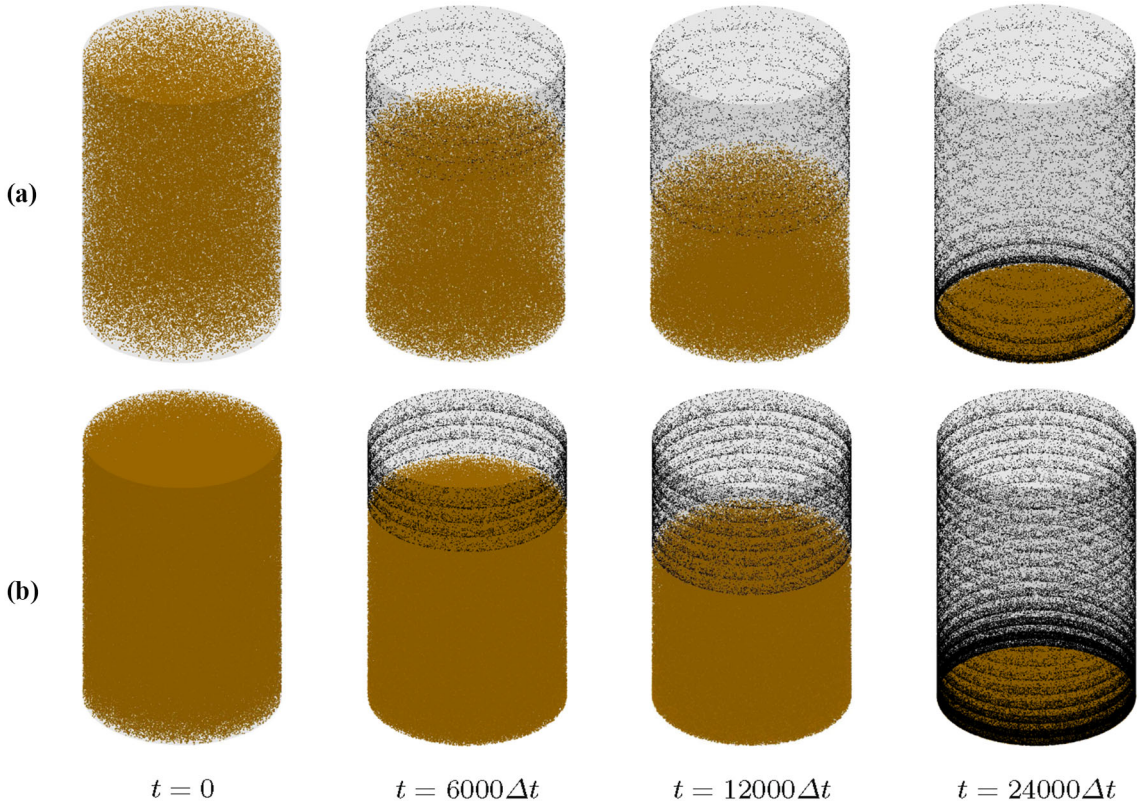

Fig. 7 Evolution of particles with the time-dependent evaporation rate in a cylindrical container. The numbers of particles are **a** $N_k = 10^5$ and **b** $N_k = 5 \times 10^5$

where $S(t)$ is a given time-dependent function and $S(0) = 3$. To simplicity of exposition, let us consider the following time-dependent evaporation rate using the sine function:

$$\frac{\mathrm{d}S(t)}{\mathrm{d}t} = -(A + \beta \sin(2\pi\gamma t)), \tag{8}$$

where A is the mean evaporation rate, β is the perturbation amplitude, and γ is the frequency. Equation (8) models effectively the time-dependent evaporation rate. We should note that we can use other forms of the time-dependent evaporation rate. The solution of Eq. (8) with the initial condition $S(0) = 3$ is given as

$$S(t) = -At + \frac{\beta}{2\pi\gamma}(\cos(2\pi\gamma t) - 1) + 3. \tag{9}$$

The parameters used are $\Delta t = 0.0001$, $\alpha = 1$, $A = 1.25$, $\beta = 3$, and $\gamma = 6$. The first (a) and second (b) rows of Fig. 7 show the evolution of particles with $N_k = 10^5$ and $N_k = 5 \times 10^5$, respectively.

Figure 8a, b shows the histogram of the pinned particles at time $t = 24000\Delta t$ with $N_k = 10^5$ and $N_k = 5 \times 10^5$, respectively. From this numerical experiment, we can clearly observe that stripe patterns are formed for both the cases.

3.4 Effect of container shape

To investigate the effect of container shape, we perform a numerical test for stripe pattern formation in a conical container with time-dependent evaporation rate using the proposed method. The time-dependent liquid domain is defined as

$$\Omega_t = \left\{ \mathbf{x} \in \mathbb{R}^3 | \sqrt{x^2 + y^2} \leq z/3 \text{ and } 0 \leq z \leq S(t) \right\}, \tag{10}$$

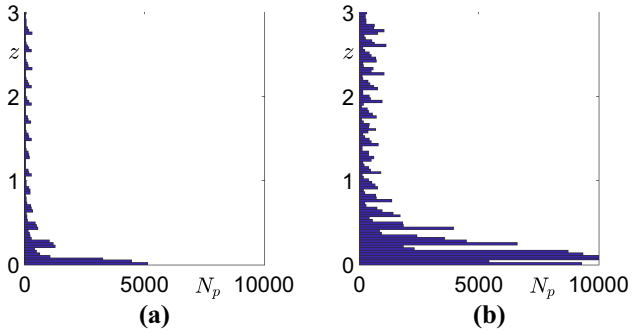

Fig. 8 Histogram of particles with respect to height at final time $t = 2400\Delta t$. The numbers of particles are **a** $N_k = 10^5$ and **b** $N_k = 5 \times 10^5$

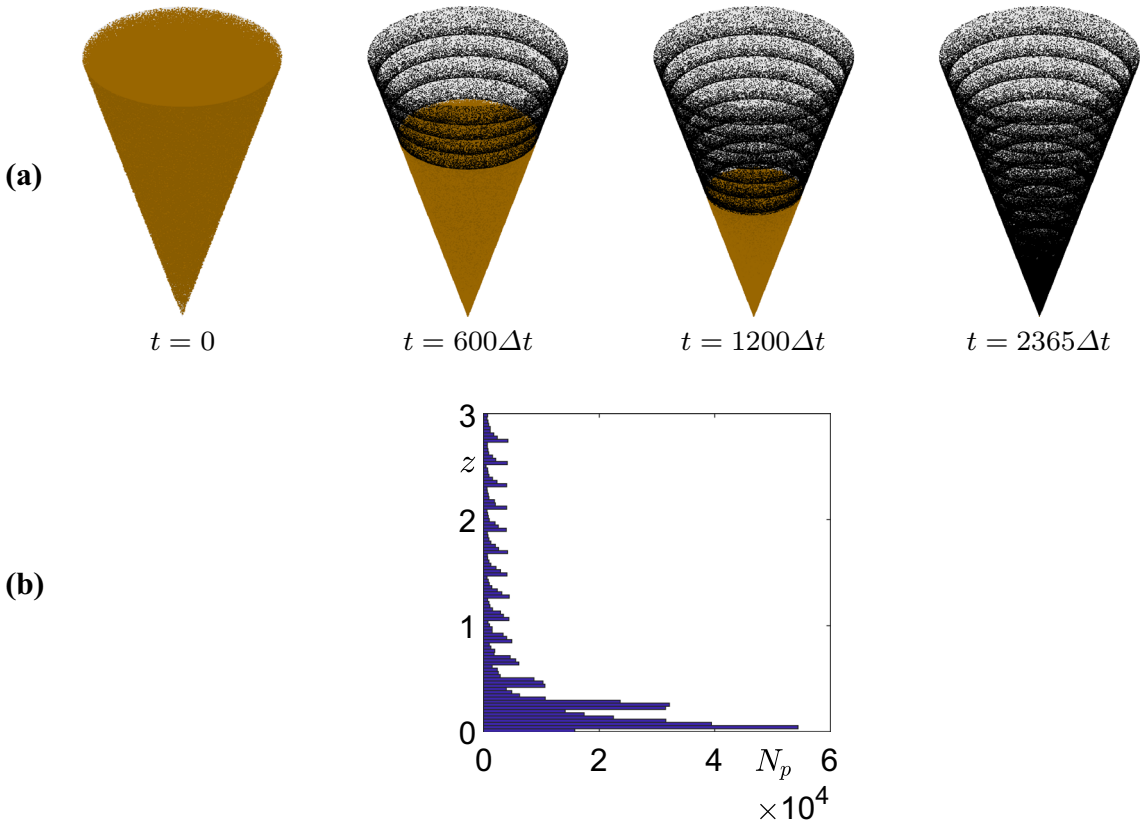

Fig. 9 **a** Evolution of particles with the time-dependent evaporation rate in a conical container. **b** Histogram of particles with respect to height at final time $t = 2365\Delta t$

where $S(t) = -At + \beta(\cos(2\pi\gamma t) - 1)/(2\pi\gamma) + 3$. The parameters used are $\Delta t = 0.001$, $\alpha = 1$, $A = 1.25$, $\beta = 3$, and $\gamma = 6$.

Figure 9a shows the temporal evolution of particles with the time-dependent evaporation rate in a conical container. Figure 9b is the histogram of particles with respect to height at final time $t = 2365\Delta t$. We can observe there is a periodic pattern of pinned particles from $z = 1$ to $z = 3$ even though the container shape is not cylindrical. The fluid surface area is getting smaller; however, there are more particles around contact lines between the fluid and container.

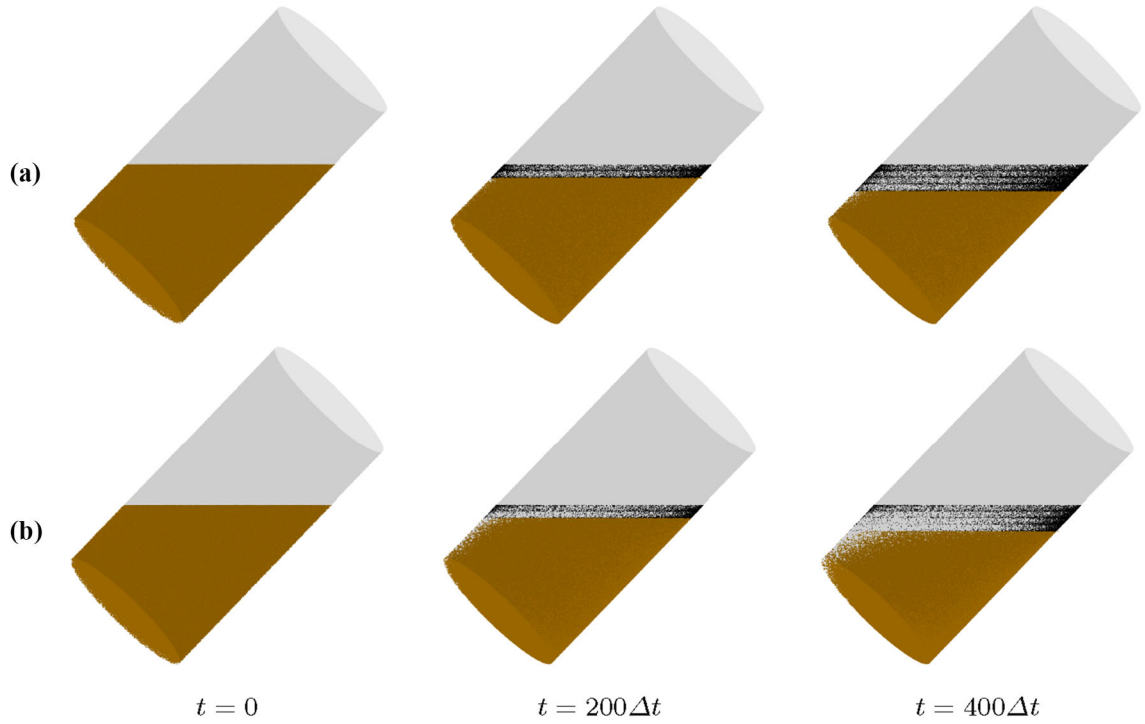

Fig. 10 Effect of gravitational parameter on the formation of coffee ring with **a** $g = 1$ and **b** $g = 2$

3.5 Effect of gravitational parameter

We investigate the effect of gravitational parameter on the coffee-ring formation inside a 45° ($\theta = \pi/4$ rad) tilted cylinder. The time-dependent tilted liquid domain is defined as follows:

$$\Omega_t = \left\{ \mathbf{x} \in \mathbb{R}^3 | \sqrt{x^2 + y^2} \leq 1 \text{ and } n_x x + n_y y + n_z (z - S(t)) \leq 0 \right\}, \tag{11}$$

where $(n_x, n_y, n_z) = \left(\cos\left(\theta + \frac{\pi}{2}\right), 0, \sin\left(\theta + \frac{\pi}{2}\right)\right)$ is a unit normal vector to the surface of the liquid and θ is the tilting angle and $S(t) = -At + \beta(\cos(2\pi\gamma t) - 1)/(2\pi\gamma) + 2$. The parameters used are $\alpha = 1$, $A = 1.25$, $\beta = 1$, and $\gamma = 10$.

The gravitational force can be written as $\mathbf{g} = (g\sin(\theta), 0, -g\cos(\theta))$. Here, for computational simplicity, we apply the tilted gravitational force instead of tilting the cylinder domain. Two different gravitational parameters are used as $g = 1$ and 2. Figure 10a, b shows the snapshots of evolution at time $t = 0, 200\Delta t$, and $400\Delta t$ with respect to $g = 1$ and 2, respectively. As we can observe, a smaller gravitational parameter causes the coffee particles to settle more slowly and more particles are pinned on the side of wall boundary. On the other hand, a larger value of gravitational parameter causes the coffee particles settle faster and the number of pinned particles on both sides of wall boundary is relatively small. Around the bottom of the container, we can also see that the coffee particles are more gathered in the tilted direction under the influence of gravity.

3.6 Effect of tilt angle

Finally, we perform the numerical simulation to study the formation of coffee ring with respect to tilt angle. We consider two different tilting angles: 10° and 55°. The time-dependent liquid domain is as follows.

$$\phi(x, y, z, t) = \begin{cases} 1 & \text{if } \sqrt{x^2 + y^2} \leq 1 \text{ and } 0 \leq z \leq S(t), \\ -1 & \text{otherwise,} \end{cases}$$

where $S(t) = -At + \beta(\cos(2\pi\gamma t) - 1)/(2\pi\gamma) + 2$. For 10° ($\theta = \pi/18$ rad) and 55° ($\theta = 11\pi/36$ rad), the gravitational force is set to $\mathbf{g} = (g\sin(\theta), 0, -g\cos(\theta))$ and the other parameter values are the same as in

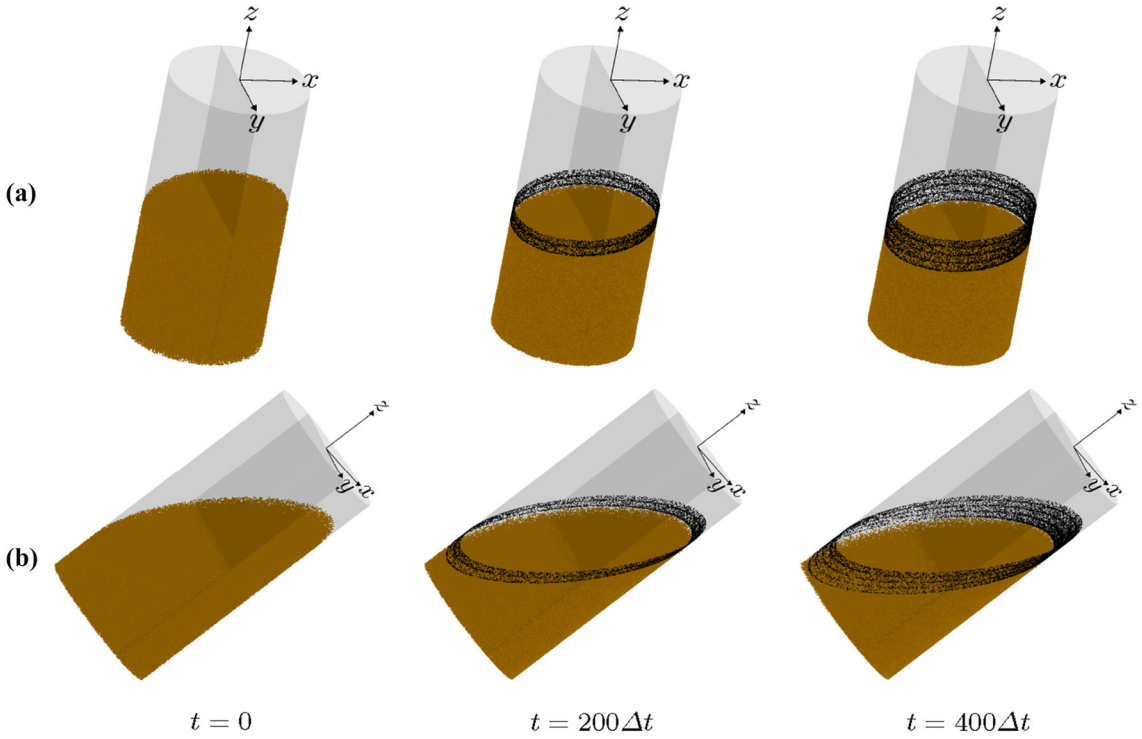

Fig. 11 Evolution of particles with a time-dependent evaporation rate in **a** 10° and **b** 55° tilted cylinders

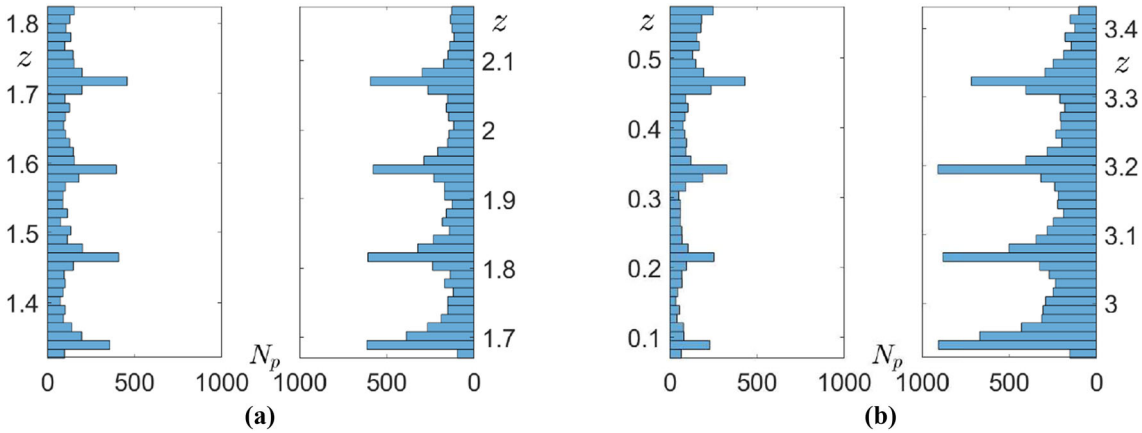

Fig. 12 Histograms of the numbers of pinned particles with respect to height at final time $t = 400\Delta t$ in **a** 10° and **b** 55° tilted cylinders

Sect. 3.5. Figure 11a, b shows the temporal evolution of particles with a time-dependent evaporation rate in 10° and 55° tilted cylinders, respectively.

Figure 12a, b shows the histograms of the numbers of pinned particles with respect to height at final time $t = 400\Delta t$ in 10° and 55° tilted cylinders, respectively. Here, the number of bins in the histograms is set to 40. The left and right histograms are the numbers of pinned particles in the area $x < 0$ and $x \geq 0$, respectively. As can be clearly observed in the histograms of Fig. 12a, b, as the angle of inclination increases, the number of particles pinned on the right contact wall increases. This phenomenon happens because coffee particles rest on the right contact wall boundary more than the right contact wall boundary.

4 Conclusions

We proposed the mathematical model for the stripe formation in a cup of coffee with a time-dependent evaporation rate. Using the Monte Carlo method, the coffee particles are defined as Lagrangian points moving under Brownian dynamics and gravity. Temporal evolution of the governing equation is solved using the explicit Euler's method. The numerical simulations were performed in the three-dimensional space. From the numerical results, we investigated that the distribution of particles and stripe pattern formations depend on the evaporation rates, the shape of container, the gravitational force, and the tilt of the cylinder. In a future work, we will use a pinning boundary condition [21] to extend the current study to investigate the hydrodynamic effect on the coffee-ring formation.

Acknowledgements The first author (Hyundong Kim) was supported by Basic Science Research Program through the National Research Foundation of Korea (NRF) funded by the Ministry of Education (NRF-2020R1A6A3A13077105). Junxiang Yang was supported by China Scholarship Council (201908260060). Chaeyoung Lee was supported by the National Research Foundation (NRF), Korea, under project BK21 FOUR. The corresponding author (J.S. Kim) was supported by Basic Science Research Program through the National Research Foundation of Korea (NRF) funded by the Ministry of Education (NRF-2019R1A2C1003053). The authors are grateful to the reviewers whose valuable suggestions and comments significantly improved the quality of this article.

Declarations

Conflict of interest The authors declare that there is no conflict of interests regarding the publication of this paper.

Data availability The datasets generated during and/or analyzed during the current study are available from the corresponding author on reasonable request.

References

1. Al-Milaji, K.N., Secondo, R.R., Ng, T.N., Kinsey, N., Zhao, H.: Interfacial self-assembly of colloidal nanoparticles in dual-droplet inkjet printing. Adv. Mater. Interfaces **5**, 1701561 (2018)
2. Deegan, R.D., Bakajin, O., Dupont, T.F., Huber, G., Nagel, S.R., Witten, T.A.: Capillary flow as the cause of ring stains from dried liquid drops. Nature **389**(6653), 827–829 (1997)
3. Whitby, C.P., Hermant, A.: Concentration of deposit patterns by nanoparticles modified with short amphiphiles. Colloids Surf. A Physicochem. Eng. Asp. **594**, 124648 (2020)
4. Yang, Q., Lv, C., Hao, P., He, F., Ouyang, Y., Niu, F.: Air bubble-triggered suppression of the coffee-ring effect. Colloid Interface Sci. Commun. **37**, 100284 (2020)
5. Devineau, S., Anyfantakis, M., Marichal, L., Kiger, L., Morel, M., Rudiuk, S., Baigl, D.: Protein adsorption and reorganization on nanoparticles probed by the coffee-ring effect: application to single point mutation detection. J. Am. Chem. Soc. **138**(36), 11623–11632 (2016)
6. Ranjbaran, M., Datta, A.K.: Retention and infiltration of bacteria on a plant leaf driven by surface water evaporation. Phys. Fluids **31**(11), 112106 (2019)
7. Poulichet, V., Morel, M., Rudiuk, S., Baigl, D.: Liquid–liquid coffee-ring effect. J. Colloid Interface Sci. **575**, 370–375 (2020)
8. Bridonneau, N., Mattana, G., Noel, V., Zrig, S., Carn, F.: Morphological control of linear particle deposits from the drying of inkjet-printed rivulets. J. Phys. Chem. Lett. **11**(12), 4559–4563 (2020)
9. Morinaga, K., Oikawa, N., Kurita, R.: Emergence of different crystal morphologies using the coffee ring effect. Sci. Rep. **8**(1), 1–10 (2018)
10. Baek, J.M., Yi, C., Rhee, J.Y.: Central spot formed in dried coffee-water-mixture droplets: inverse coffee-ring effect. Curr. Appl. Phys. **18**(4), 477–483 (2018)
11. Lian, H., Qi, L., Luo, J., Zhang, R., Hu, K.: Uniform droplet printing of graphene micro-rings based on multiple droplets overwriting and coffee-ring effect. Appl. Surf. Sci. **499**, 143826 (2020)
12. Zhang, D., Gao, B., Chen, Y., Liu, H.: Converting colour to length based on the coffee-ring effect for quantitative immunoassays using a ruler as readout. Lab. Chip **18**(2), 271–275 (2018)
13. Miller, J.B., Usselman, A.C., Anthony, R.J., Kortshagen, U.R., Wagner, A.J., Denton, A.R., Hobbie, E.K.: Phase separation and the 'coffee-ring' effect in polymer–nanocrystal mixtures. Soft Matter **10**(11), 1665–1675 (2014)
14. Wen, J.T., Ho, C.M., Lillehoj, P.B.: Coffee ring aptasensor for rapid protein detection. Langmuir **29**(26), 8440–8446 (2013)
15. Mampallil, D., Eral, H.B.: A review on suppression and utilization of the coffee-ring effect. Adv. Colloid Interface Sci. **252**, 38–54 (2018)
16. Crivoi, A., Duan, F.: Three-dimensional Monte Carlo model of the coffee-ring effect in evaporating colloidal droplets. Sci. Rep. **4**, 4310 (2014)
17. Kim, H.S., Park, S.S., Hagelberg, F.: Computational approach to drying a nanoparticle-suspended liquid droplet. J. Nanopart. Res. **13**(1), 59–68 (2011)
18. Crivoi, A., Duan, F.: Elimination of the coffee-ring effect by promoting particle adsorption and long-range interaction. Langmuir **29**(39), 12067–12074 (2013)

19. Xu, T., Lam, M.L., Chen, T.H.: Discrete element model for suppression of coffee-ring effect. Sci. Rep. **7**, 42817 (2017)
20. Yang, J., Kim, H., Lee, C., Kim, S., Wang, J., Yoon, S., Kim, J.: Phase-field modeling and computer simulation of the coffee-ring effect. Theor. Comput. Fluid. Dyn. **34**(5), 679–692 (2020)
21. Lee, H.G., Yang, J., Kim, J.: Pinning boundary conditions for phase-field models. Commun. Nonlinear Sci. Numer. Simul. **82**, 105060 (2020)